International Journal of Precision Engineering and Manufacturing (2026)
SMART TECHNOLOGY
Online ISSN 2951-6382
Print ISSN 2951-4614
REGULAR PAPER

Quasi-Static, Rolling and Shear Behaviors of an Auxetic Non-Pneumatic Tire with TPMS-Based Spokes

Hong-Seok Kim[1] · Do-Yeon Kim[2] · Sang-Hu Park[3]

Received: 5 March 2026 / Revised: 18 April 2026 / Accepted: 22 April 2026 / Published online: 22 April 2026

Abstract

This study investigates the quasi-static rolling behavior and shear response of a non-pneumatic tire incorporating a Triply Periodic Minimal Surface (TPMS)-based Rotated Primitive Auxetic Structure (RPAS). The RPAS spoke derives a negative Poisson's ratio from rotational transformations of Primitive TPMS unit cells, enabling load-adaptive variable stiffness through auxetic densification. Building upon validated static results, quasi-static rolling simulations over approximately 2.7 spoke-pitch cycles showed that position-dependent ground reaction force fluctuations were reduced to 0.78% for the RPAS, compared to 3.32% for a conventional honeycomb design at 2.5 mm compression. This reduction is attributed to a self-compensating mechanism where auxetic densification of the RPAS partially bridges the geometric gaps between discrete spokes. Shear analysis yielded a stiffness of 0.61 N/mm for the RPAS, comparable to the honeycomb tire (0.58 N/mm), indicating that the auxetic architecture does not compromise longitudinal stability. These numerical insights provide a foundation for future investigations involving multi-cycle loading and high-speed dynamics to further extend the scalability of the proposed RPAS design. The present findings should be interpreted as structural design tendencies obtained under quasi-static numerical conditions; extension to high-speed operation and full-scale rubber tires requires dedicated experimental and viscoelastic-dynamic validation.

Keywords Airless tire · Triply periodic minimal surface · Auxetic structure · Variable stiffness · Rolling stability

✉ Sang-Hu Park
sanghu@pusan.ac.kr

[1] Research Institute of Mechanical Technology, Pusan National University, Busan 46241, Republic of Korea
[2] Graduate School of Mechanical Engineering, Pusan National University, Busan 46241, Republic of Korea
[3] School of Mechanical Engineering, Pusan National University, Busan 46241, Republic of Korea

1 Introduction

Pneumatic tires have long served as the dominant wheel technology owing to their superior load-carrying capacity, vibration damping, and non-linear progressive stiffness that provides soft compliance at small deformations and increasing resistance under heavy loads [1,2]. However, their reliance on compressed air introduces inherent vulnerabilities, including punctures, blowouts, and the necessity for continuous pressure monitoring, posing significant safety and maintenance concerns in demanding operational environments [3,4]. Non-pneumatic tires (NPTs) address these fundamental limitations by replacing the air-filled cavity with compliant spoke or lattice structures, offering a maintenance-free, puncture-proof alternative particularly suited for military, agricultural, construction, and autonomous vehicle applications [5,6].

The mechanical performance of NPTs is primarily governed by the spoke architecture, which must simultaneously satisfy the conflicting requirements of load-carrying capacity, lateral stability, and ride comfort [7]. Honeycomb structures have been widely adopted for their high specific stiffness and energy absorption [8,9]; however, many conventional lattice designs exhibit linear elastic responses followed by abrupt buckling or plateau regions, fundamentally differing from the smooth non-linear stiffness curve of pneumatic tires [10,11]. Auxetic lattice geometries, exhibiting a negative Poisson's ratio (NPR), have recently attracted considerable attention for their unique densification behavior under compression, which can potentially replicate the progressive stiffness characteristics of pneumatic systems [12,13]. Nevertheless, translating auxetic behavior into functional NPT spokes while ensuring structural stability over the full deformation range remains a significant engineering challenge.

Triply Periodic Minimal Surfaces (TPMS) offer a promising design framework for NPT spokes, featuring smooth continuous geometries that minimize stress concentrations while providing exceptional stiffness-to-weight ratios and energy absorption

https//doi.org/10.57062/ijpem-st.2026.00080

capabilities [14,15]. Kim et al. [16] demonstrated that Primitive-type TPMS (P-TPMS) cells, when configured as cylindrical spokes, exhibit nearly linear force vs. displacement behavior up to 60.8% strain—substantially outperforming conventional column, honeycomb, and re-entrant cells that show typical lattice behavior characterized by linear, plateau, and densification regions. Building upon this foundation, Kim et al. [17] proposed a Rotated Primitive-based Auxetic Structure (RPAS) derived by applying rotational transformations to P-TPMS unit cells, thereby inducing auxetic behavior. The RPAS tire exhibited variable stiffness depending on the deformation state: higher rigidity through densification when compressed on flat ground and obstacles, a characteristic advantageous for shock absorption and prevention of large local deformations. Lee et al. [18] further advanced TPMS-based NPT spoke design by introducing spiral subdivision for asymmetric cell embedment, enabling adaptive control of directional stiffness under driving and braking conditions.

A critical review of the existing literature reveals that NPT research has been overwhelmingly focused on uniaxial compression tests, static finite element analyses, and parametric design studies [19,20]. These quasi-static approaches, while valuable for fundamental design validation, do not capture the complex dynamic phenomena encountered during actual rolling operation, where transient loading, ground contact migration, and cyclic deformation at varying speeds significantly influence tire performance [21]. This gap is particularly pronounced for auxetic-structured NPTs: although the RPAS concept has been thoroughly validated under static compression and obstacle loading [17], its behavior in rolling tire systems — where spokes undergo cyclic compression and release at varying rotational positions — has received virtually no attention. Crucially, it remains unknown whether the auxetic self-densification mechanism, which delivers variable stiffness under quasi-static loading, can also suppress the position-dependent reaction force (RF) fluctuations that are an inherent limitation of discrete spoke architectures. Furthermore, while the shear stability of conventional NPT designs has been investigated [9], the longitudinal shear behavior of auxetic TPMS-based tires under combined vertical pre-compression and longitudinal displacement loading remains largely unexplored, leaving a critical gap in multi-axial performance assessment.

To the best of the authors' knowledge, the quasi-static rolling behavior and longitudinal shear response of an auxetic TPMS-based NPT have not been previously reported. Building upon the static compressive framework established in [17], the present study addresses this gap through: (i) numerical characterization of position-dependent ground reaction force fluctuations during quasi-static rolling and the role of auxetic densification in their suppression; (ii) examination of how compression level governs RF fluctuation magnitude; and (iii) evaluation of the longitudinal shear response under sequentially applied vertical pre-compression and longitudinal shear displacement. A conventional honeycomb NPT is used as the comparison baseline throughout.

2 RPAS Design and Finite Element Modeling

The Rotated Primitive-based Auxetic Structure (RPAS) was developed by applying a rotational transformation to a Primitive-type Triply Periodic Minimal Surface (P-TPMS) unit cell, the geometry of which is governed by Eq. (1) [22]:

$$\emptyset_P = \cos\left(\frac{2\pi x}{L}\right) + \cos\left(\frac{2\pi y}{L}\right) + \cos\left(\frac{2\pi z}{L}\right) - a\left(\cos\left(\frac{2\pi x}{L}\right)\cos\left(\frac{2\pi y}{L}\right) + \cos\left(\frac{2\pi y}{L}\right)\cos\left(\frac{2\pi z}{L}\right) + \cos\left(\frac{2\pi z}{L}\right)\cos\left(\frac{2\pi x}{L}\right)\right) + c \quad (1)$$

where L is the unit cell length, c is the level-set constant controlling the volume fraction, a is a shape constant, and x, y, z are the coordinate values. As illustrated in **Fig. 1**, the RPAS is generated through three sequential steps: (1) rotating the P-TPMS unit cell by angle θ about the diagonal h-axis, (2) applying a Boolean intersection with a bounding box to ensure inter-cell connectivity, and (3) arraying the processed cells in three-dimensional space. This rotational transformation converts the inherently positive Poisson's ratio of the P-TPMS into a NPR, endowing the RPAS with an auxetic densification mechanism under compressive loading.

All finite element analyses (FEA) were conducted in ANSYS (2020 R2) using the Yeoh 3rd-order hyperelastic model, whose parameters were calibrated from uniaxial tensile tests on the PolyJet photopolymer Elastico (Stratasys J55 Prime) following ASTM D-412. The fitted material constants of the Yeoh model are C_{10} = 0.076 MPa, C_{20} = 0.296 MPa, and C_{30} = 0.029 MPa. A comprehensive parametric study using an L9 orthogonal array over the three design parameters (θ, a, L) established that L = 20 mm, a = 0.4, and θ = 10° yields an optimal balance of negative Poisson's ratio, vertical stiffness, and energy absorption for airless tire spoke applications [17]. The level-set constant c was determined to achieve the target volume fraction (VF = 0.49). These design parameters and material constants are adopted throughout the present study. Full details of the unit cell design, material characterization, parametric optimization, and mesh convergence study are reported in [17]. The mesh size of 1 mm adopted in the present rolling and shear analyses follows the converged configuration established therein. It should be noted that the Yeoh law used here represents the PolyJet photopolymer employed for small-scale prototype validation in [17]; Mullins softening, strain-rate-dependent viscoelasticity, and reinforcement effects present in fiber-reinforced rubber compounds are not captured. Consequently, the absolute stiffness and RF values reported in Sections 3.2–3.3 should be interpreted in a comparative sense — i.e., as structural design tendencies between RPAS and honeycomb — rather than as quantitative predictions for production rubber tires. Future work targeting full-scale geometries will adopt a Prony-series viscoelastic model combined with a fiber-reinforced rubber constitutive law to enable direct comparison with pneumatic baselines.

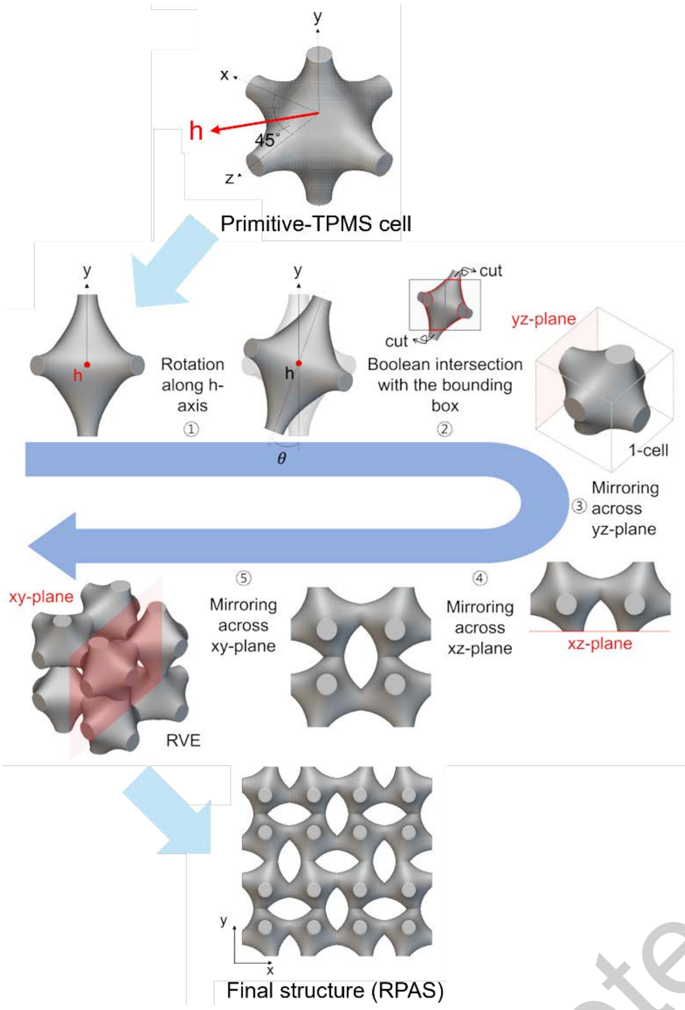

Fig. 1 Design process of variable stiffness structure named RPAS. Adapted from Kim et al. [17], licensed under CC BY 4.0 (http://creativecommons.org/licenses/by/4.0/).

3 Static and Dynamic Behavior of RPAS Tire

3.1 Static Behavior of Tire

In all analyses presented in this study, a honeycomb tire serves as the reference structure. The honeycomb is the most widely adopted NPT spoke architecture [8,9,21,22], and shares an identical volume fraction (VF = 0.49) and material (PolyJet Elastico) with the RPAS tire, isolating the architectural difference — positive versus negative Poisson's ratio — as the primary variable. Comparison with alternative auxetic architectures (e.g., re-entrant) is left for future work, as equivalent small-scale fabrication and rolling data are not yet available in the literature.

To provide a baseline for the subsequent dynamic and shear analyses, the static compressive behavior of the RPAS and honeycomb tires is briefly summarized here; full experimental and numerical details are reported in [17]. Both tires were fabricated at small scale using the PolyJet photopolymer Elastico, with identical volume fractions (VF = 0.49), inner ring diameter of 108 mm, and outer ring diameter of 162 mm. The RPAS spoke consists of 22 circumferential cells and 2 radial layers, while the honeycomb spoke uses 16 circumferential cells with a cell wall thickness of 3.1 mm, as shown in **Fig. 2(a)**.

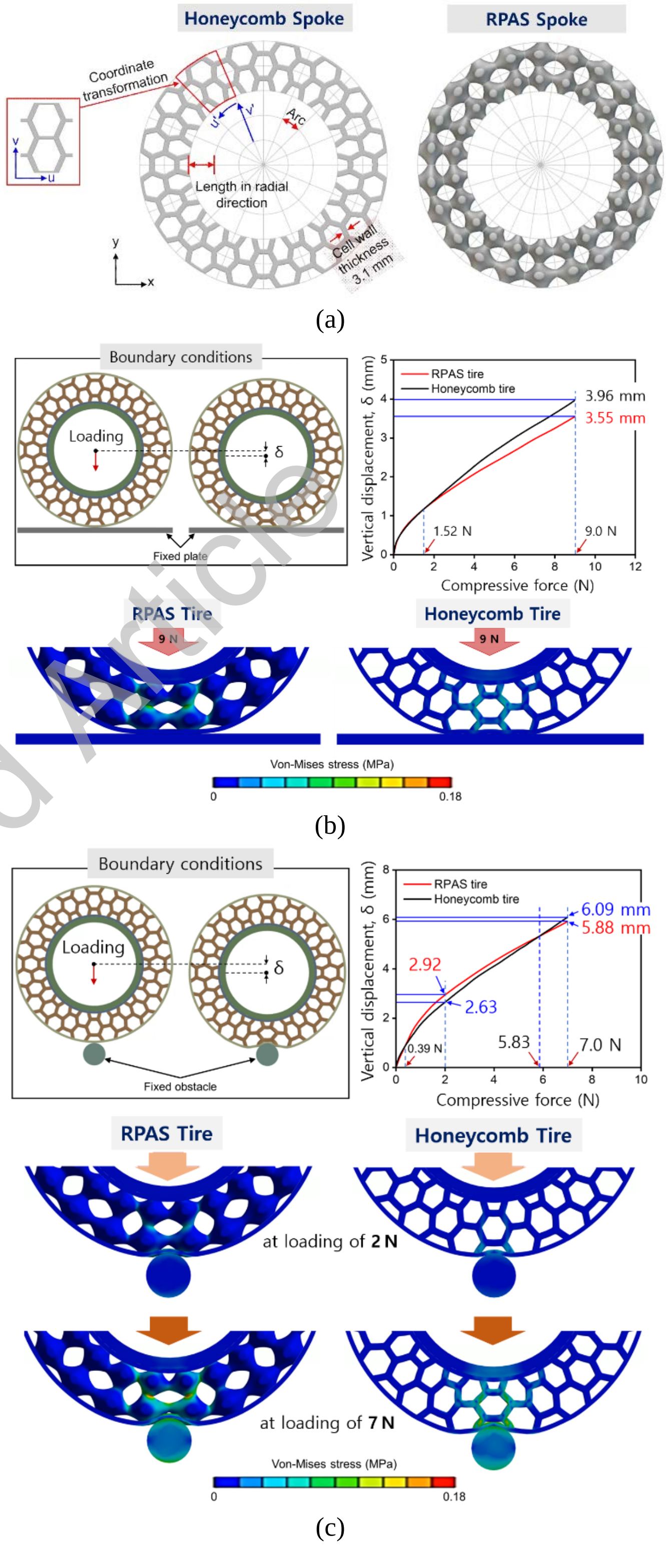

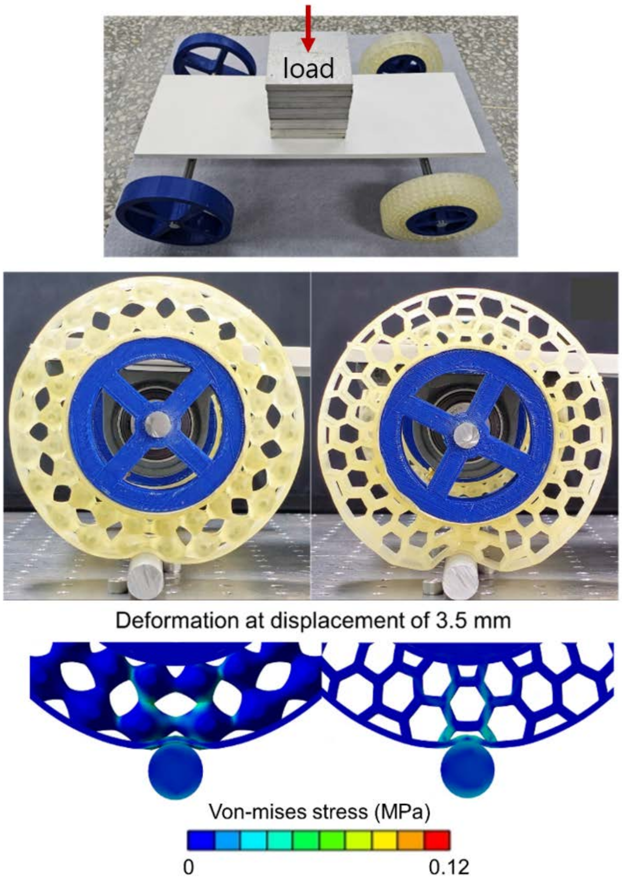

(d)

Fig. 2 (a) Comparison of the dimensions of two airless tire models. (b-c) Deformation of two tires on flat surface and obstacle. (d) Experiment setup for measuring deformation behavior of two tires and analysis results at loading condition for displacement of 3.5 mm. Adapted from Kim et al. [17], licensed under CC BY 4.0 (http://creativecommons.org/licenses/by/4.0/).

Under flat-surface compression, the RPAS tire showed a non-linear progressive stiffening response with a 10.4% reduction in vertical displacement at 9 N compared to the honeycomb tire (**Fig. 2(b)**). A crossover at approximately 1.52 N separates a compliant low-load regime from a progressively stiffer high-load regime driven by auxetic densification. Under obstacle loading, the RPAS tire produced a 3.4% reduction in vertical displacement at 7 N (**Figs. 2(c)-(d)**). These static results provide the baseline for the rolling and shear analyses in Sections 3.2 and 3.3.

3.2 Quasi-static Rolling Behavior of Tire

Figure 3(a) illustrates the boundary conditions for the quasi-static rolling simulation. The tire was initially compressed against a rigid flat surface by a prescribed vertical displacement δ, after which the rigid surface was rotated at an angular velocity of 0.01745 rad/s for 45°, a rotation range covering approximately 2.7 spoke-pitch cycles of the RPAS tire (360° / 22 circumferential cells ≈ 16.4° per cell), thereby ensuring that nearly three complete periodic units of the position-dependent RF variation are captured in the analysis window.

The low rotational velocity (0.01745 rad/s, corresponding to a linear surface speed of ~1.4 mm/s at the outer radius) was selected to isolate position-dependent geometric effects from inertial and centrifugal contributions, the latter being negligible at this speed ($\omega^2 R \approx 2.5 \times 10^{-5}$ m/s² ≪ g). Accordingly, the present simulations are conducted under quasi-static velocity conditions. The objective is not to characterize high-speed inertial behavior addressed in [21] but to quantify the cyclic ground RF variation arising from the sequential engagement of discrete spoke units, a structural transient phenomenon absent in quasi-static compression analyses. High-speed effects including centrifugal force and viscoelastic energy dissipation, which may partially counteract the auxetic inward contraction at elevated speeds, are reserved for future investigation. For reference, a typical passenger-tire operating condition of 60 km/h at $R \approx 300$ mm corresponds to $\omega \approx 56$ rad/s, at which the centrifugal acceleration ($\omega^2 R \approx 9.3 \times 10^2$ m/s²) exceeds gravity by roughly two orders of magnitude and becomes a dominant loading contribution. Aerodynamic drag, though geometry- and speed-dependent, similarly grows with v^2 and is not negligible at highway speeds. Accordingly, the quasi-static values reported herein are expected to shift in both magnitude and trend when these effects are incorporated. A dedicated explicit-dynamic analysis combined with rolling-drum experimentation is planned as the immediate follow-up study to characterize the speed-dependent evolution of the self-compensating mechanism identified here. Consequently, the quantitative RF fluctuation values reported herein should be interpreted as indicative of the geometric self-compensating trend rather than as predictions of performance under realistic operating speeds.

Numerical reliability of the present rolling and shear analyses inherits from the mesh convergence study reported in [17], in which the element size adopted here (1 mm) was identified as the converged configuration for the same RPAS and honeycomb geometries. The constitutive law (Yeoh 3rd-order), element type, and material constants are preserved unchanged between the static validation in [17] and the rolling/shear simulations presented here; only the boundary and contact conditions are adapted to each loading scenario. At the adopted rotational velocity (0.01745 rad/s), inertial contributions are negligible relative to the elastic restoring forces as discussed above, so the simulation regime remains quasi-static throughout. Consistent with standard practice in NPT numerical studies [19,21], the present analyses are therefore intended to reveal structural design tendencies — the direction and relative magnitude of the performance changes induced by the auxetic architecture — rather than to predict absolute values under real driving conditions.

The internal structural response during rotation is presented in the dynamic stiffness profiles in **Fig. 3(b)**. Both tires exhibited periodic stiffness fluctuations, but the RPAS tire demonstrated a significantly wider operational stiffness bandwidth and higher sensitivity to compression levels (δ = 1.5, 2.0, and 2.5 mm). Interestingly, while the RPAS exhibited larger instantaneous stiffness fluctuations (ΔK) compared to the honeycomb, its final output—the ground RF in **Fig. 3(c)**—showed superior uniformity. This result is attributed to the stiffness sensitivity of the auxetic cells, which undergo densification more readily than honeycomb cells as compression increases. This transition from bending to a densified stretching-dominated mode may partially bridge the geometric gaps between spokes, reducing the net RF variation at the ground contact.

In contrast, the honeycomb tire's periodic force fluctuations originate from the positional variation in its internal cell architecture. The number of horizontal cell walls within the contact zone varies with the rotational position of the tire: positions where two horizontal walls are engaged exhibit substantially higher load-carrying resistance than positions where only a single horizontal wall is present. This is because the horizontal walls act as geometric constraints that suppress the lateral expansion of the inclined cell walls under compression. The mechanism therefore depends on the local wall count and spacing at each rotational position, so the effective stiffness varies in a deterministic, position-dependent manner. The resulting position-dependent stiffness profile is directly reflected in the periodic oscillations of the ground RF shown in **Fig. 3(b) and 3(c)**, a structural limitation that cannot be resolved through simple parameter tuning.

The RF variation is defined as (RF_max − RF_min) / RF_mean × 100%, where RF_max, RF_min, and RF_mean are the maximum, minimum, and mean ground reaction forces recorded over the 45° rotation period, respectively. As summarized in **Fig. 3(d)**, the honeycomb tire exhibits increasing RF fluctuation with compression level, while the RPAS shows the opposite trend: RF variation decreases progressively with δ, reaching 0.78% at δ = 2.5 mm compared to 3.32% for the honeycomb — a 76.5% reduction. This divergent trend is consistent with the hypothesis that higher compression promotes greater auxetic densification, enhancing the load redistribution capacity of the RPAS and strengthening the self-compensating mechanism at deeper deformation states. These results suggest that the RPAS may become inherently more stable under heavier operational loads, a characteristic advantageous for applications where tire deformation varies with vehicle weight and road conditions.

A qualitative basis for the self-compensating mechanism can be framed in terms of how each architecture discretizes the ground-contact arc. At matched outer diameter, the RPAS engages a larger number of circumferential spoke cells than the honeycomb (22 vs 16), providing a finer angular discretization of the contact zone and, as a consequence, a smaller step change in the effective stiffness each time the contact patch transitions from one cell to the next. This discretization effect alone, however, does not fully account for the divergent trends in **Fig. 3(d)**: the RPAS RF fluctuation decreases with δ, whereas the honeycomb RF fluctuation increases. The difference originates in the deformation mode of the loaded cell. Beyond the compression level at which auxetic densification is activated, each loaded RPAS cell transitions from a bending-dominated to a stretching-dominated response and recruits its immediate neighbors through the transverse inward contraction characteristic of negative Poisson's ratio behavior, so that the load applied to one cell is partially redistributed to adjacent cells and the discrete cell-to-cell stiffness steps are smoothed out. The honeycomb cell, which has no equivalent lateral-contraction mechanism, cannot redistribute load across neighboring cells and therefore retains a stiffness profile that remains modulated by the discrete count of horizontal walls within the contact zone — a behavior that is intensified rather than suppressed as δ increases. The divergent trend in **Fig. 3(d)** is thus a direct consequence of this cell-to-cell load-sharing capability, not merely of the circumferential cell count.

The practical significance of this finding should be interpreted within the scope of the present numerical study. The reported RF variation values were obtained under quasi-static rolling conditions using a small-scale photopolymer model, and their quantitative applicability to full-scale tires at operational speeds remains to be established. The self-compensating mechanism is rooted in a geometric principle — the ratio of contact-zone cell count to total spoke count — which scales proportionally with tire diameter: from 22 cells at 162 mm to approximately 84 cells at 600 mm, maintaining a comparable cell size of ~20 mm. This geometric similarity supports the hypothesis that the mechanism would remain operative at full scale. However, full-scale implementations involve different material systems, manufacturing processes, and loading magnitudes, and a dedicated full-scale numerical and experimental study is required to quantify the scaling behavior. Experimental validation on full-scale rubber prototypes, including rolling-resistance, durability, and spoke-level deformation measurements under representative road conditions, is planned as the direct follow-up to this numerical study. These experiments lie outside the scope of the present paper but constitute the immediate next phase of the project.

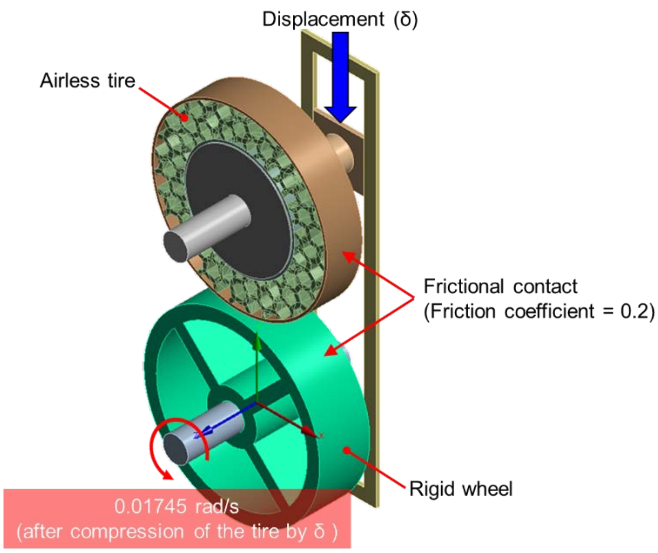

(a)

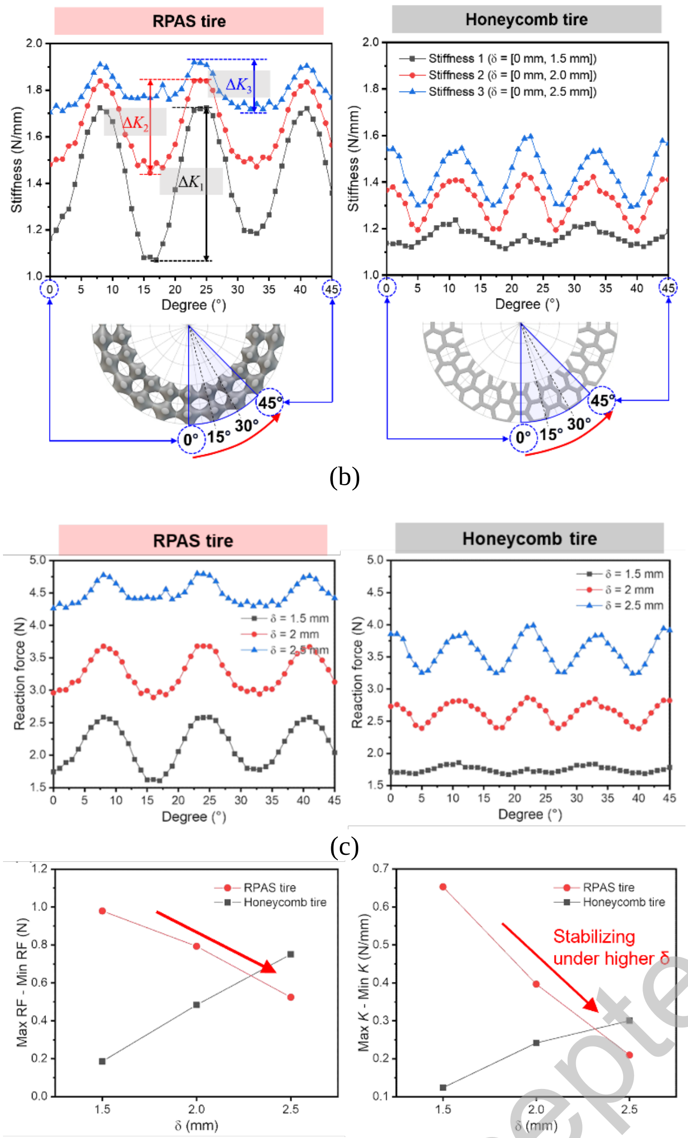

Fig. 3 Numerical evaluation of quasi-static rolling behavior and dynamic stability. (a) Schematic of simulation boundary conditions and sequential two-step analysis procedure. (b) Dynamic stiffness fluctuations and (c) ground reaction force profiles over a 45° rotation period for varying compression levels (δ). (d) Quantitative summary of maximum and minimum dynamic responses across different displacements, highlighting the self-stabilizing effect and superior operational uniformity of the RPAS.

The structural basis of the self-compensating mechanism of the RPAS tire is directly visualized in **Fig. 4**. **Fig. 4(a)** presents the von Mises stress distributions of the RPAS tire lattice structure at four rotational positions (0°, 15°, 30°, and 45°), viewed from the front. The localized stress concentration at individual unit cell joints appears consistent across all rotational positions, suggesting that the densification onset is relatively position-independent. The structural contrast between the two architectures is further shown in **Fig. 4(b)**, which presents an oblique view of the spoke lattice stress distributions for both tire structures at 30° rotation. In the honeycomb tire, stress is broadly distributed across multiple horizontal cell walls, with the magnitude and pattern varying depending on how many walls are engaged at a given rotational position — the mechanistic origin of its position-dependent RF fluctuation. In contrast, the RPAS tire exhibits highly localized stress concentration at individual unit cell joints, characteristic of auxetic densification onset, enabling efficient load redistribution across the spoke structure regardless of rotational position.

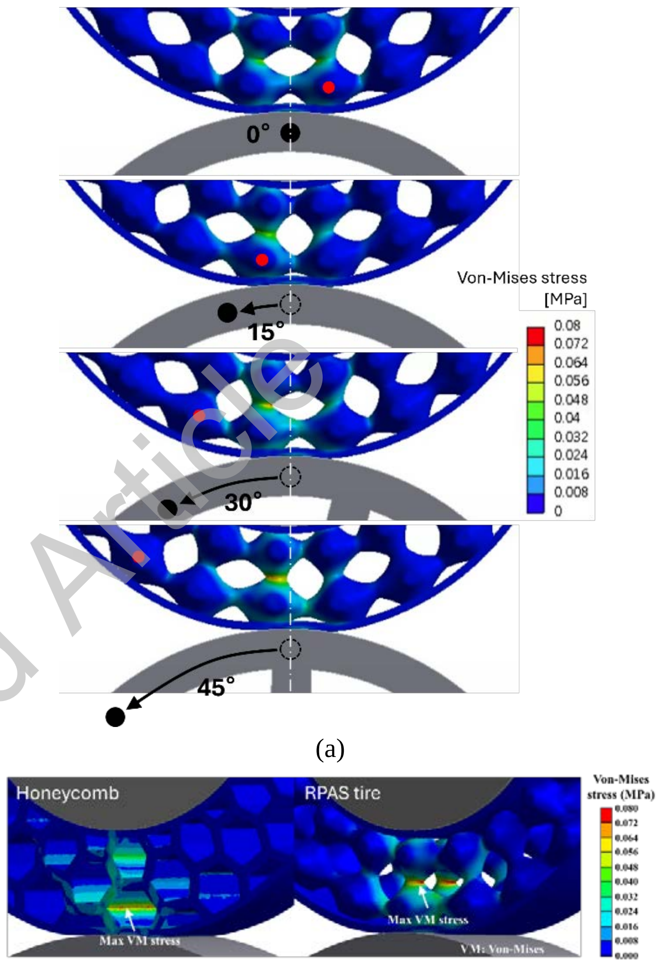

Fig. 4 (a) Front-view stress distributions of the RPAS tire at four rotational positions (0°, 15°, 30°, and 45°), demonstrating the position-independent consistency of the localized stress concentration at unit cell joints. (b) Oblique-view comparative stress distributions of the honeycomb (left) and RPAS (right) tire lattice structures at 30° rotation; white arrows indicate maximum stress locations.

3.3 Analysis of Shear Stability of Tire

To evaluate the structural robustness under longitudinal shear loading representative of acceleration and braking conditions, the shear characteristics of the airless tires were investigated. As illustrated in Fig. 5(a), the simulation was conducted in two sequential steps. First, the tire was compressed to a vertical displacement of 2.5 mm — the level at which the RPAS achieves maximum dynamic uniformity as demonstrated in Section 3.2. A longitudinal displacement of 3 mm was then applied, selected to remain within the linear shear response regime of both tire structures while capturing the initial shear stiffness characteristics relevant to the longitudinal loading encountered during braking and acceleration maneuvers. A bonded contact condition was applied between the tread and the rigid plate to isolate the intrinsic shear resistance of the spoke structure from frictional sliding effects at the interface.

Fig. 5(b) presents the von Mises stress distribution under shear loading. Both structures exhibited stress patterns similar to those observed under vertical compression, yet their deformation mechanisms differed. In the honeycomb tire, stress concentrations were localized along the inclined walls of the hexagonal cells. For the RPAS tire, stress was primarily concentrated at the joints connecting the unit cells. Notably, the volume contraction (auxetic effect) was not observed during shear deformation. This suggests that the rotated primitive geometry is optimized for axial densification rather than lateral shear-induced contraction, indicating a decoupled mechanical response between vertical and longitudinal loading.

The limited influence of the RPAS architecture on shear stiffness can be understood from the geometric character of the rotated primitive cell. Auxetic densification under axial loading originates from the rotation of the P-TPMS cell by angle θ about the diagonal h-axis, which introduces coupling between the loading direction and the transverse direction, so that radial compression drives transverse inward contraction (NPR). Under longitudinal shear, however, the loading axis is not aligned with this rotation plane, and the shear deformation is accommodated primarily by bending and rotation of the inter-cell joints rather than by volumetric contraction; the dominant coupling responsible for auxetic densification is therefore not activated. The resulting shear stiffness is governed by local joint-bending behavior common to both architectures, which accounts for the comparable values measured in **Fig. 5(c)**. This vertical–lateral decoupling is an intrinsic characteristic of the rotated primitive geometry rather than a shortcoming: the RPAS delivers variable vertical stiffness without compromising the shear load-path relevant to cornering and braking stability.

The bonded tread–ground interface adopted in the present shear simulation isolates the intrinsic shear resistance of the spoke lattice from frictional effects at the contact patch. Under realistic braking, a Coulomb friction law would permit interface slip once the tangential force exceeds the product of the friction coefficient and the normal load, potentially reducing the apparent shear stiffness and introducing stick–slip transients that are absent from the present idealization. The bonded assumption therefore provides an upper-bound estimate of the intrinsic spoke shear stiffness, which is conservative for the comparative architecture assessment pursued here (RPAS vs honeycomb) and is a standard idealization for isolating structural response from interface effects in NPT spoke-design studies. A dedicated friction-contact analysis incorporating a Coulomb law and a rubber–asphalt contact description is planned alongside the high-speed rolling study, to quantify the extent to which interface slip dissipates the longitudinal load-carrying capacity implied by the intrinsic stiffness reported here.

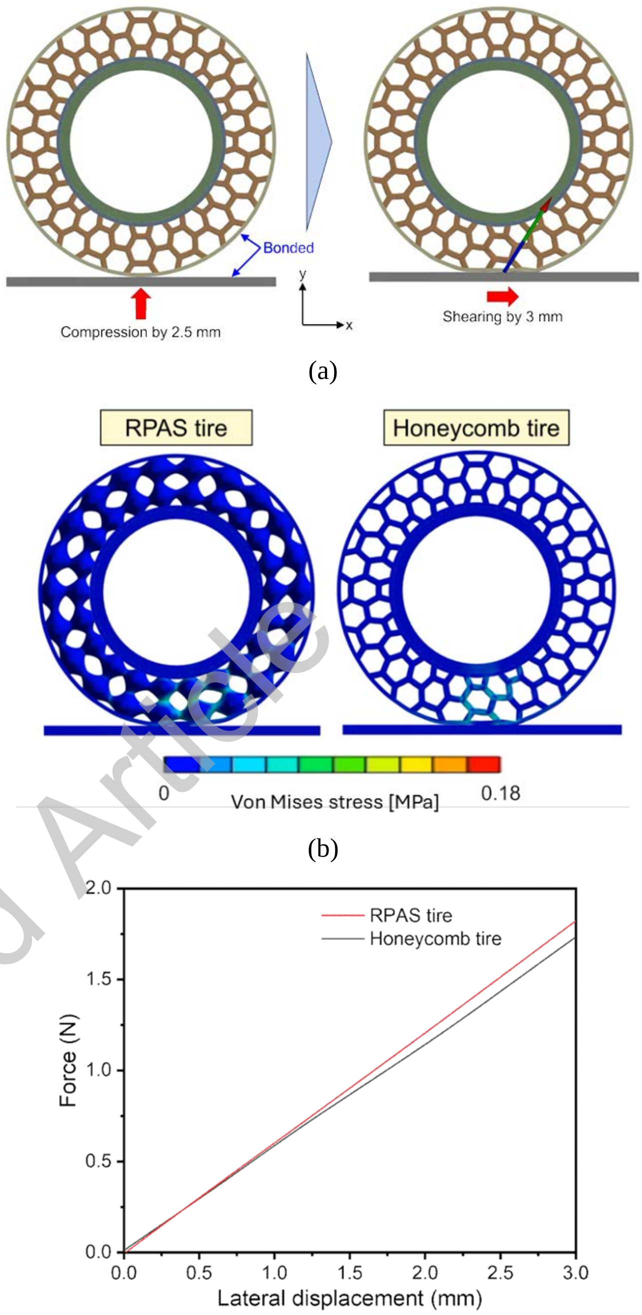

(c)

Fig. 5 (a) Numerical boundary conditions for shear analysis, featuring a 2.5 mm vertical pre-compression followed by a 3 mm lateral displacement. (b) Comparison of von Mises stress distributions under shear. (c) Shear load-displacement curves, where the RPAS tire demonstrates a shear stiffness of 0.61 N/mm, providing comparable longitudinal stability to the conventional honeycomb tire (0.58 N/mm).

The shear load-displacement curves in **Fig. 5(c)** show that the RPAS tire achieves a shear stiffness of 0.61 N/mm, effectively equivalent to the honeycomb tire (0.58 N/mm); the nominal 5% difference is within the range of numerical uncertainty and should not be interpreted as a meaningful performance distinction. In light of prior findings that honeycomb NPTs already provide sufficient shear stiffness relative to pneumatic counterparts [23], the present results confirm that the RPAS constitutes a viable alternative that preserves shear competitiveness while offering the additional benefits of auxetic densification under vertical and rolling loading [17].

Direct experimental validation of the rolling and shear simulations has not been performed in this study. The FE framework — material constants, mesh, and contact settings — was validated against static compression and obstacle loading experiments in [17], and the present simulations adopt the same constitutive model and mesh parameters with boundary conditions adapted to each loading scenario. Several limitations should be noted beyond those discussed in Sections 3.2. The bonded contact condition in the shear analysis excludes frictional sliding at the tread–ground interface, which may lead to overestimation of intrinsic shear stiffness under realistic braking and acceleration conditions. Additionally, extrapolating a statically validated hyperelastic model to rolling and shear scenarios introduces uncertainty regarding strain-rate effects, contact transients, and interface behavior that cannot be fully assessed without dedicated dynamic experiments. Experimental characterization including dynamic force measurements and digital image correlation (DIC) under rolling conditions is identified as a priority for future work.

4 Conclusions

This paper presented a numerical investigation of the quasi-static rolling stability and shear response of an airless tire incorporating a Rotated Primitive-based Auxetic Structure (RPAS), benchmarked against a conventional honeycomb-structured tire. Building upon the static design framework established in [17], the principal findings are summarized as follows:

(1) Quasi-static rolling simulations over approximately 2.7 spoke-pitch cycles revealed that the RPAS tire reduces position-dependent RF fluctuations to 0.78% at $\delta = 2.5$ mm — a 76.5% reduction relative to the honeycomb (3.32%). This suppression is attributed to the auxetic densification mechanism, which redistributes contact loads across geometric discontinuities between discrete spokes. The effect strengthens with increasing compression level, suggesting inherently greater stability under heavier operational loads.

(2) The RPAS tire achieved a shear stiffness of 0.61 N/mm, comparable to the honeycomb tire (0.58 N/mm). The nominal 5% difference is within the range of numerical uncertainty and is interpreted as indicating equivalent rather than superior shear performance — consistent with the design intent of the RPAS, whose auxetic architecture is optimized for axial densification rather than lateral shear resistance.

The present results provide numerical evidence that a TPMS-based auxetic spoke architecture can suppress position-dependent RF fluctuations while maintaining competitive shear stability. These findings are subject to the limitations of a quasi-static, small-scale photopolymer model, and quantitative generalization to full-scale rubber tires at realistic operating speeds requires dedicated experimental and high-speed numerical validation. As illustrated in **Fig. 6**, a full-scale 600 mm RPAS tire has been conceptualized as a direction for future work, alongside high-speed rolling simulations and experimental characterization via dynamic force measurement and DIC.

Limitations and future work. The scope of the present numerical study is delimited by the following assumptions: (i) all rolling and shear analyses were performed under quasi-static velocity (ω = 0.01745 rad/s), so inertial, centrifugal, aerodynamic, and viscoelastic-dissipation effects relevant to high-speed operation are excluded; (ii) the Yeoh hyperelastic law, calibrated on a PolyJet photopolymer, does not represent the Mullins softening, strain-rate sensitivity, or fiber reinforcement present in production rubber compounds, so the reported force values should be interpreted as comparative design tendencies between RPAS and honeycomb rather than as absolute predictions for rubber tires; (iii) the shear analysis employed a bonded tread–ground contact and therefore provides an upper-bound estimate of the intrinsic spoke shear stiffness, excluding frictional slip; and (iv) direct experimental validation of rolling and shear behavior was not performed in the present study — the constitutive law, mesh density, and FE framework were previously validated against static compression and obstacle loading in [17]. Priority directions for future work are: (a) explicit-dynamic high-speed rolling simulations incorporating centrifugal and viscoelastic effects; (b) rolling and shear experiments on full-scale rubber prototypes with instrumented force and strain measurement; (c) multi-cycle fatigue and rolling-resistance characterization under representative road conditions; and (d) coupled friction-contact analysis using a Coulomb friction law to quantify the impact of interface slip on longitudinal load-carrying capacity during braking.

Fig. 6 Conceptual design of a full-scale RPAS tire with an outer diameter of 600 mm, composed of four unit cells in the radial direction.

Acknowledgement(s)

This work was supported by the Basic Research Support Program of Pusan National University during 2025-2026 (2 years).

References

1. Gent, A. N., & Walter, J. D. (2006). The pneumatic tire. *National Highway Traffic Safety Administration.*
2. Pacejka, H. B. (2012). Tire and vehicle dynamics, 3rd edition.

Butterworth-Heinemann.

3. Dixon, J. C. (1996). Tires, suspension and handling, 2nd edition. *Society of Automotive Engineers*.
4. Rhyne, T. B., & Cron, S. M. (2006). Development of a non-pneumatic wheel. *Tire Science and Technology*, 34(3), 150–169.
5. Sardinha, M., Fátima Vaz, M., Ramos, T. R., & Reis, L. (2023). Design, properties, and applications of non-pneumatic tires: A review. *Proceedings of the Institution of Mechanical Engineers, Part L: Journal of Materials: Design and Applications*, 237(11), 2277–2297.
6. Ju, J., Kim, D. M., & Kim, K. (2012). Flexible cellular solid spokes of a non-pneumatic tire. *Composite Structures*, 94(8), 2285–2295.
7. Aboul-Yazid, A. M., Emam, M. A., Shaaban, S., & El-Nashar, M. A. (2015). Effect of spokes structures on characteristics performance of non-pneumatic tires. *International Journal of Automotive and Mechanical Engineering*, 11, 2212–2223.
8. Jin, X., Hou, C., Fan, X., Sun, Y., Lv, J., & Lu, C. (2018). Investigation on the static and dynamic behaviors of non-pneumatic tires with honeycomb spokes. *Composite Structures*, 187, 27–35.
9. Ju, J., & Kim, D. M. (2011). Compliant hexagonal periodic lattice structures having both high shear strength and high shear strain. *Materials & Design*, 32(2), 512–524.
10. Gibson, L. J., & Ashby, M. F. (1997). Cellular solids: Structure and properties, 2nd edition. *Cambridge University Press*.
11. Ingrole, A., Hao, A., & Liang, R. (2017). Design and modeling of auxetic and hybrid honeycomb structures for in-plane property enhancement. *Materials & Design*, 117, 72–83.
12. Lakes, R. S. (1987). Foam structures with a negative Poisson's ratio. *Science*, 235(4792), 1038–1040.
13. Ren, X., Das, R., Tran, P., Ngo, T. D., & Xie, Y. M. (2018). Auxetic metamaterials and structures: A review. *Smart Materials and Structures*, 27(2), 023001.
14. Al-Ketan, O., & Abu Al-Rub, R. K. (2019). Multifunctional mechanical metamaterials based on triply periodic minimal surface lattices. *Advanced Engineering Materials*, 21(10), 1900524.
15. Maskery, I., Sturm, L., Aremu, A. O., Panesar, A., Williams, C. B., Tuck, C. J., Wildman, R. D., & Ashcroft, I. A. (2018). Insights into the mechanical properties of several triply periodic minimal surface lattice structures made by polymer additive manufacturing. *Polymer*, 152, 62–71.
16. Kim, H. S., Kim, D. Y., Choi, J. W., & Park, S. H. (2024). High stability in compressive and shear behavior of airless tire using Primitive TPMS-based cylindrical spoke. *International Journal of Precision Engineering and Manufacturing-Green Technology*, 11(4), 1247–1262.
17. Kim, D. Y., Kim, H. S., Kamath, S. S., Hou, X., Choi, J. W., & Park, S. H. (2024). TPMS-based auxetic structure for high-performance airless tires with variable stiffness depending on deformation. *Scientific Reports*, 14(1), 11419.
18. Lee, J. W., Oh, S. H., & Kim, D. W. (2025). Optimal design of TPMS-based non-pneumatic tire spoke with adaptive directional stiffness. *International Journal of Precision Engineering and Manufacturing-Green Technology*, 1-15.
19. Rugsaj, R., & Suvanjumrat, C. (2020). Study of geometric effects on nonpneumatic tire spoke structures using finite element method. *Mechanics Based Design of Structures and Machines*, 50(7), 2379–2399.
20. Andriya, N., Dutta, V., & Vani, V. V. (2022). Study on 3D printed auxetic structure-based non-pneumatic tyres (NPT'S). *Materials and Manufacturing Processes*, *37*(11), 1280-1297.
21. Rugsaj, R., & Suvanjumrat, C. (2021). Dynamic finite element analysis of rolling non-pneumatic tire. *International Journal of Automotive Technology*, 22(4), 1011–1022.
22. Zheng, X., Guo, X., & Watanabe, I. (2021). A mathematically defined 3D auxetic metamaterial with tunable mechanical and conduction properties. *Materials & Design*, *198*, 109313.
23. Zhang, Z., Fu, H., Liang, X., Chen, X., & Tan, D. (2020). Comparative analysis of static and dynamic performance of nonpneumatic tire with flexible spoke structure. *Stroj. Vestn. J. Mech. Eng*, 66, 458-466.

Hong-Seok Kim

received his Ph.D. in the School of Mechanical Engineering, Pusan National University. He is currently a postdoctoral researcher at the Research Institute of Mechanical Technology, Pusan National University. His research interests include laser-directed energy deposition (L-DED), in-situ process monitoring, and metal matrix composites.

Do-Yeon Kim

is a master graduate student in School of Mechanical Engineering at Pusan National University. His research interests include design for additive manufacturing (DfAM) and auxetic materials.

Sang-Hu Park

is a Professor in the School of Mechanical Engineering, and an Executive Vice President for External Affairs and Strategy at Pusan National University. Also, he is a director, Center for Hybrid Innovative Manufacturing & Engineering (Core Facility). His research fields are design for additive manufacturing and processes.